Published in final edited form as:
Chembiochem. 2012 May 7; 13(7): 1039–1045. doi:10.1002/cbic.201200034.

Multimodal interventional molecular imaging of tumor margins and distant metastases by targeting the $\alpha_v\beta_3$ integrin

Dr. Anton Bunschoten[a],[b],+, **Tessa Buckle, BS**[a],[b],+, **Nils Visser, BS**[c], **Dr. Joeri Kuil**[a],[b], **Dr. Hushan Yuan**[d], **Dr. Lee Josephson**[d], **Dr. Alexander L. Vahrmeijer**[e], and **Dr. Fijs W.B. van Leeuwen.**[a],[b]

Fijs W.B. van Leeuwen.: F.W.B.van_Leeuwen@lumc.nl

[a]Department of Radiology, Leiden University Medical Center, 2300 RC Leiden, The Netherlands, (+31)71 5248256 [b]Division of Diagnostic Oncology, The Netherlands Cancer Institute – Antoni van Leeuwenhoek Hospital, 1066 CX Amsterdam, The Netherlands [c]Division of Experimental Therapy, The Netherlands Cancer Institute – Antoni van Leeuwenhoek, Hospital, 1066 CX Amsterdam, The Netherlands [d]Centre for Translational Nuclear Medicine and Molecular Imaging, Massachusetts General Hospital / Harvard Medical School, MA 02129, Charlestown, USA [e]Department of Surgery, Leiden University Medical Center, 2300 RC Leiden, The Netherlands

Abstract

$\alpha_v\beta_3$ Integrin is involved in (tumor induced) angiogenesis and is a promising candidate for the specific visualization of both primary tumors and their distant metastases. Combining radioactive and fluorescent imaging labels in a single multimodal or rather hybrid RGD-based imaging agent enables integration of pre-, intra- and postoperative angiogenesis imaging. A hybrid imaging agent targeting the $\alpha_v\beta_3$ integrin, ^{111}In-MSAP-RGD, which contains a targeting moiety, a DTPA chelate and a cyanine dye, was evaluated for its potential value in combined lesion detection and interventional molecular imaging in a 4T1 mouse breast cancer model. SPECT/CT and fluorescence imaging were used to visualize the tumor in vivo. Tracer distribution was evaluated ex vivo down to the microscopic level. The properties of ^{111}In-MSAP-RGD were compared to those of ^{111}In-DTPA-RGD. Biodistribution studies revealed a prolonged retention and increased tumor accumulation of ^{111}In-MSAP-RGD compared to ^{111}In-DTPA-RGD. Using ^{111}In-MSAP-RGD identical features of the tumor could be visualized preoperatively (SPECT/CT) and intraoperatively (fluorescence imaging). Next to the primary tumor, ^{111}In-MSAP-RGD also enabled detection and accurate excision of distant metastases in the head and neck region of the mice. The hybrid RGD-derivative ^{111}In-MSAP-RGD shows potential in preoperative planning and fluorescence based surgical intervention.

Keywords

Multimodal imaging; Imaging agents; Angiogenesis; Surgical guidance; Fluorescence

Correspondence to: Fijs W.B. van Leeuwen., F.W.B.van_Leeuwen@lumc.nl.

+These authors contributed equally to this work.

Supporting information for this article is available on the WWW under http://www.chembiochem.org or from the author.

Introduction

In the rapidly advancing field of molecular imaging a large variety of new imaging agents are emerging,[1] most of which are designed to visualize tumor-specific biomarkers and detect tumors preoperatively in a non-invasive manner. Despite the recent advances in probe development, the best success story for preoperative clinical lesion detection so far is the untargeted ^{18}F-FDG, a small and fairly general agent for the imaging of increased (tumor) metabolism that can be applied to detect a wide variety of tumor types.[2] Unfortunately, ^{18}F-FDG is not tumor specific and also accumulates in other areas with increased metabolism. Detection of tumor cells using specific targets on these cells may be a promising addition to the clinical field of molecular imaging. A possible example of such a method is targeting of tumor-induced angiogenesis e.g. by using the already well-validated "small" cyclic Arg-Gly-Asp (RGD) peptide-derivatives. These small peptides bind to the transmembrane $\alpha_v\beta_3$ integrins, which are mainly expressed on activated endothelial cells involved in angiogenesis.[3, 4] Besides detection of cancerous lesions, integrin-targeting imaging agents might also be of value in other applications in which angiogenesis is part of the pathophysiological process, for instance in atherosclerosis, vulnerable plaque formation, inflammatory and infectious processes.[5-9]

Fluorescence based surgical guidance is an extension of molecular imaging into the field of surgery, that can also be called interventional molecular imaging.[10] Currently, clinical fluorescence guidance is predominantly confined to visualization of sentinel lymph nodes using (untargeted) dyes such as indocyanine green (ICG) or methylene blue.[11, 12] For targeted clinical fluorescence imaging only the metabolic tumor activity imaging with 5-aminolevulinic acid (5-ALA),[13] and more recently FITC-folate for the detection of ovarian cancer have been reported.[14] 5-ALA is clinically used in visualizing superficial and brain tumors e.g. glioblastoma,[13] where the red emission can be accurately seen on top of the gray brain mass.[15] Folate targeted imaging was explored in folate receptor-alpha over-expressing tumors like ovarian, renal, lung and breast cancer,[16] and was used to detect sub millimeter metastases. The success of these relatively small tumor targeted imaging agents might well be linked to their complete and rapid circulation. It would be interesting to study the small RGD-derivatives, as a potential third clinical imaging probe for interventional molecular imaging of tumors and their (distant) metastases demonstrating tumor-induced angiogenesis.

Combining detection orientated and interventional molecular imaging widens the applicability of both approaches. Multimodal or rather hybrid imaging agents can combine the best characteristics of two modalities.[17] Previously we have shown that hybrid imaging agents, which are both radioactive and fluorescent, allow for integrated diagnostics of the (sentinel) lymph nodes receiving drainage directly from the tumor.[18, 19] In this concept, the radioactive signal is used to visualize the lesion preoperatively and to plan the surgical intervention accordingly (Fig. 1 and movie supplement of ref 20). The fluorescent beacon, on the other hand, is used to provide optical surgical fluorescence guidance. Next to the preclinical validation this concept has also proven its added value in clinical sentinel node procedures.[20-22] Similarly, this hybrid imaging technology platform can also be extrapolated to targeted imaging applications with e.g. peptides,[23] antibodies,[24] and diabodies.[25] In this line of reasoning, a hybrid RGD-derivative is most desirable serving the advantages of preoperative nuclear imaging and intraoperative fluorescence imaging in one targeted imaging agent. Such a probe could also be applied in *ex vivo* pathological evaluation of excised specimens to identify tumor tissue and validate tumor free excision margins. Although, a number of such multimodal RGD-derivatives have already been reported in literature,[26-30] to the best of our knowledge so far none has been studied for their potential in surgical guidance and combined pre- and intraoperative imaging.

In the current study we evaluate the feasibility of combining pre-, intra- and postoperative angiogenesis imaging using a targeted hybrid approach (Fig. 1). Here fore, the hybrid imaging agent ^{111}In-MSAP-RGD was generated and its ability to visualize tumor lesions was assessed in a mouse model for breast cancer.

Results

Based on the well-validated cyclic RGD-pentapeptide [31, 32] we synthesized a DTPA-RGD analogue, similar to a peptide of which the efficacy in tumor imaging was previously demonstrated by van Hagen et al.[33] For multimodal detection a hybrid derivative, MSAP-RGD, was synthesized (Scheme 1). In the latter, only the diagnostic label is different; the MSAP label contains a cyanine dye on top of the DTPA chelate (Scheme 1), which fluoresces in the near infrared (NIR) region. The hybrid MSAP-RGD derivative is still capable of binding to $\alpha_v\beta_3$-expressing cells selectively as determined by FACS analysis (see Fig. SI1). Both the DTPA-RGD and MSAP-RGD derivatives allow for accurate detection of 4T1 tumors Balb/c nude mice using SPECT/CT (Fig. 2).

The biodistribution was evaluated according to “standard” radioisotope analysis using the radioactive label of both ^{111}In-DTPA-RGD and ^{111}In-MSAP-RGD (Table 1). Fluorescence based biodistribution measurements will be influenced by the limited tissue penetration of the fluorescent signal and by the background fluorescence, e.g. autofluorescence of tissue and chow, as shown by tissue autofluorescence measurements of untreated mice (Fig. SI2). Especially the intestine and stomach will be largely influenced by the autofluorescence. The distribution data show that both imaging agents accumulate significantly in the tumor compared to other organs. Although the relative distribution of both imaging agents is approximately the same, the MSAP derivative shows, on average, a factor 10 higher %ID/g at 24 hr post injection in most tissues. Nevertheless, this higher background signal did not diminish the quality of the SPECT/CT image (Fig. 2) because the tumor/muscle ratios are almost identical for both the DTPA- (11.11 ± 4.16) and MSAP-derivative (9.03 ± 3.81). Consequently the increase in retention does not appear to alter the specificity of the RGD-peptide. The biodistribution shows a relative high %ID/g for e.g. the lungs, nevertheless this large low-density organ is not causing significant background signal in the SPECT/CT (Fig. 2).

To study the link between the increased retention of MSAP-RGD and the possible interactions of the fluorescent dye with albumin, the biodistribution of albumin was determined using ^{99m}Tc-Vasculosis (see SI) (Table 1, excluding tumor). At 24h the ratio found for ^{99m}Tc-Vasculosis and MSAP-RGD was 1.4±0.8 (average of all measured organs excluding tumor and blood, a ratio of 1 would mean complete overlap) while the ratio of ^{99m}Tc-Vasculosis with DTPA-RGD was 16.2±10.2. This similarity indicates involvement of HSA in the distribution of MSAP-RGD.

At microscopic level the same hybrid probe could be visualized in fresh tumor tissue by confocal microscopy after iv injection of MSAP-RGD (Fig. 4B). The biodistribution of the tracer could also be visualized by *ex vivo* fluorescent imaging of the organs, resulting in high signals from the primary tumor, metastases, kidneys and liver (Fig. 3C and SI3). A drawback of this method is the high (auto)fluorescence signal from the intestine and stomach, which originates (mainly) from the chow (Fig. SI2). For this reason, these organs are covered in Figure 3B. None or very low fluorescence was observed from the (coagulated) blood, brain, heart, lungs, spleen, muscle, mammary fat pad and lymph nodes (Fig. SI3).

The added value of the RGD-based multimodal surgical guidance approach becomes most apparent when applied to animals with distant metastases in the head and neck region. The SPECT/CT image shows, first of all, the primary tumor as a dark spot surrounded by a ring of activity (approx. 15 × 11 mm)(Figure 3A). Therefore, fluorescence imaging will visualize especially tumor margins, which is exactly what is surgically required. As the tumor rim shows the highest blood vessel density (Figure 4A), the rim contains significant amounts of the RGD probe. The high vascularization in this area was confirmed using FITC-lectin perfusion experiments and CD31 fluorescence immunohistochemistry. IHC confirmed that the primary tumor had a necrotic core (Fig. SI4), which is in agreement with the low functional blood vessel density in the core. *Ex vivo* fluorescence microscopy of the excised tissue confirmed that the accumulation of MSAP-RGD was most abundant in the well-vascularized outer rim of the tumor (Figure 4B). As such the primary tumor margins are illuminated (Figure 3B and C).

Due to tissue attenuation of the fluorescent signal, the metastases (Figure 3A) could initially not be detected using fluorescence imaging alone. Guided by the preoperative SPECT/CT image it was, however, possible to locate the metastases via fluorescence imaging after removal of overlying tissue. Subsequently, all five metastases (approx. 3 × 3 mm) situated in the head and neck area of the animal could be excised. Pathologic analysis confirmed the presence of tumor cells in these excised tissue specimens (Fig. S4B).

Discussion

By using a multimodal derivative of RGD (^{111}In-MSAP-RGD) we have expanded our hybrid surgical guidance concept to a targeted approach using angiogenesis imaging. It is well known and established that cancer outgrowth and the formation of distant metastases is led, among other phenomena, by hypoxia and angiogenesis.[34] It was previously shown that RGD peptides retain their affinity for $\alpha_v\beta_3$ integrin after functionalization with a hybrid optical and nuclear imaging label, which is structurally similar to that of our reported MSAP label.[27] MSAP-RGD binds also to $\alpha_v\beta_3$-expressing cells specifically after conjugation to the MSAP label (Fig. SI1).

As we have previously shown for sentinel lymph node procedures, the added value of the hybrid approach over conventional fluorescence imaging lies in the ability to accurately plan surgery by pre-operative visualization. In this case ^{111}In-MSAP-RGD allows the detection of the primary tumor (i.e. primarily visualization of the tumor margins) and its distant metastases using SPECT/CT imaging (Fig. 1 and 3).

In our recent review on multimodal tumor targeted peptides we found that “large” multimodal quantum dots and dendrimer-based imaging agents functionalized with RGD-peptides had difficulties extravasating and subsequently targeting of tumors and had a very negative influence on the biodistribution.[23, 35, 36] This underlines that the optimal multimodal label should be small to facilitate rapid and complete distribution and should, preferably, only consist of the two imaging labels on a small scaffold. However, “small” (peptidic) imaging agents generally show fast (renal) clearance limiting the time to bind to its target and limiting the time for the preoperative imaging, surgical planning and the actual surgical intervention. To overcome this mismatch, non-covalent interactions with a biological carrier molecule might be used to improve the retention of the small imaging agent. It has previously been shown that peptides labeled with cyanine dyes, such as the one present on the MSAP label, can interact with albumin, thereby influencing the pharmokinetics of the agent in the body.[37, 38] The addition of the cyanine dye resulted indeed in an increased retention of MSAP-RGD compared to the DTPA-RGD, most likely because of its non-covalent interaction with albumin. At 24h the distribution ratios of

MSAP-RGD and ^{99m}Tc-albumin (Vasculosis) are highly similar (excluding blood and tumor). We previously demonstrated that competing binding sites could easily break the non-covalent interactions between cyanine dyes and HSA. Therefore we reason that albumin merely acts as a carrier molecule and as such, alters the pharmacokinetics of MSAP-RGD. When the MSAP-RGD guest molecules are exposed to an alternative binding site, they will thus be striped of the initial albumin-carrier molecules (Fig. 5). Consequently, it can be expected that the amount of MSAP-RGD in the blood is no longer in relation to the amount of ^{99m}Tc-Vasculosis at 24 hours. The interactions between MSAP-RGD and albumin might explain the increase in general retention and the increase in signal from the tumor. The increased uptake improves the signal retention yielding a higher fluorescence signal from the target lesions. The similar T/M ratios indicate preservation of the $\alpha_v\beta_3$-integrin specific uptake of the hybrid agent. As intra-operative fluorescence imaging may be less sensitive than nuclear imaging this increase in retention may aid in fluorescence based identification of the target lesions during the surgical intervention.

The added value of the multimodal RGD peptide over a mono-functionalized DTPA-derivative is showcased in Figure 1 and 4. Herein we depict the preoperative planning and orientation followed by intra-operative fluorescence imaging of the same compound (^{111}In-MSAP-RGD) *in vivo*. Although mono functionalized ^{111}In-DTPA-RGD would allow a surgeon to delineate where the tumor is in a 3D-SPECT/CT image (clinical resolution up to 10 mm), due to the lack or real-time feedback it would not allow surgical navigation to its precise location. It would also not allow visualization of the tumor margins during surgery. Overall, this would make it especially difficult to excise small clustered metastases as those found in the head and neck area of the mice (Fig. 3). On the other hand, our clinical experience has taught us that the tissue attenuation of a (NIR) fluorescent signal will not enable detection of lesions located deeper than one centimeter. The limited tissue penetration of fluorescent signals is, however, beneficial for approaching the tumor and its margins in the cm-mm range. Moreover, as we have found in a clinical setting, the limited tissue penetration of fluorescence ensures shielding of fluorescent background signals.[20, 21] Unless a tumor is directly associated with the liver or kidneys, the auto-fluorescence, as observed in mice (Fig. SI2 and SI3) is not expected to be problematic in the translation of this technology to humans.

Applying each single-modality technique by itself might result in an incomplete tumor/metastases excision. The multimodal hybrid approach, however, combines the advantages of the two individual techniques and enables accurate 3D identification of the primary tumor and its metastases (Fig. 1-3), while supporting the surgeon to accurately navigate towards the suspected lesions and offering diagnostics to the pathologist (Fig. 4). By using the hybrid technology we preserve the current standard of care (i.e. nuclear medicine for surgical planning) and add to this an additional feature of fluorescence detection.[39] Because of the navigation based on nuclear imaging, the application of our hybrid approach does not depend on the tissue penetration of the fluorescent emission. This may create the possibility to use fluorescent dyes that emit in the visible range in a hybrid imaging approach.

The wide application of angiogenesis/integrin imaging,[9] suggest MSAP-RGD is a promising candidate for further development and perhaps even clinical translation. It could supplement the already clinically validated hybrid imaging agent (ICG-^{99m}Tc-NanoColl) for integrated surgical guidance.[20, 21] Moreover, conceptually it would also pave the way for other tumor targeted peptides or small conjugates e.g. those that target the chemokine receptor 4 (CXCR4).[40, 41]

Conclusion

Tumors at the implantation site and small tumor foci distal to implantation ("metastases") were successfully detected by SPECT/CT (pre-operatively) and by fluorescence imaging (intra-operatively) after iv injection of the multimodal MSAP-RGD reagent. This strategy most likely would result in improved margin delineation, and improved detection and resection of metastases.

Experimental Section

General

NMP, DCM, DMF, CH_3CN, MTBE, hexanes (AR-S grade) and TFA (peptide synthesis) were obtained from Biosolve (Valkenswaard, The Netherlands). DTPA(*t*Bu)$_4$ was purchased from Macrocyclics (Dallas, USA). Protected amino acids and PyBop were purchased from Novabiochem (Merck, Darmstadt, Germany). TIS, HFIP, HOBt, DMSO, BOP and DIPEA were obtained from Sigma-Aldrich (Zwijndrecht, The Netherlands). TentaGel S TRT-Gly-Fmoc was obtained from Rapp Polymere (Tübingen, Germany). Animals received standard chow, as we previously observed that this does not influence the clinical translation of hybrid imaging agents wherein a radiolabel can be used to monitor the distribution.[18-20]

RGD

c[RGDfK] was synthesized by solid phase peptide synthesis using a trityl resin (Tentagel S TRT-Gly-Fmoc) and applying the Fmoc/*t*Bu strategy with PyBop as coupling reagent. The protected peptide was cleaved from the resin with 20% HFIP in DCM and was cyclized with BOP/HOBt/DIPEA. After deprotection with 95% TFA/2.5% TIS/2.5% water and precipitation in MTBE/hexanes the peptide was purified by preparative HPLC using a Waters HPLC system with a UV detector operating at 220 nm and a Waters Atlantis C18 10 μm (250 × 19 mm) column. A gradient of 0.1% TFA in H_2O/CH_3CN 95:5 to 0.1% TFA in H_2O/CH_3CN 5:95 in 40 minutes was used. The product was obtained as a white fluffy solid after pooling of the appropriate fractions and lyophilization.

MSAP

The multifunctional single attachment point reagent (MSAP), containing a Cy5.5 derivative (CyAL-5.5b, λ_{ex}= 674 nm; λ_{em}= 693 nm)[42] and a DTPA-chelate, was synthesized according to previously described procedures.[40, 43]

MSAP-RGD

c[RGDfK] (1.24 mg, 1.5 μmol) and the MSAP-reagent (1.0 mg, 0.6 μmol) were dissolved in DMSO (400 μL). DIPEA (5 μL, 30 μmol) was added and the mixture was stirred overnight at room temperature, after which the product was purified by preparative HPLC as described above. (Scheme 1) The product was obtained as a blue fluffy solid (1.2 mg, 84 %) after pooling of the appropriate fractions and lyophilization. MS (MALDI-TOF): $[M+H]^+$ calculated for $C_{102}H_{138}N_{19}O_{28}S_3$: 2172.9, found 2172.9.

DTPA-RGD

DTPA(*t*Bu)$_4$ (4.1 mg, 6.6 μmol), NHS (0.76 mg, 6.6 μmol) and DCC (1.36 mg, 6.6 μmol) were dissolved in DMF (1 mL) and stirred for 30 min. Next c[RGDfK] (5 mg, 6 μmol) and DIPEA (2 μL, 12 μmol) were added and the reaction was stirred overnight. After concentration in vacuo, the product was deprotected with 95% TFA/2.5% TIS/2.5% water and purified by preparative HPLC as described above. (Scheme 1) The product was obtained

as a white fluffy solid (2.4 mg, 36%) after pooling of the appropriate fractions and lyophilization. MS (ESI): $[M+H]^+$ calculated for $C_{41}H_{63}N_{63}O_{16}$: 979.4, found 978.7.

Radiolabeling

For radiolabeling, MSAP-RGD (40 μg, 18 nmol) or DTPA-RGD (25 μg, 25 nmol) was dissolved in 0.1M acetic acid (50 μL) and $^{111}InCl_3$ (110 MBq/ 300 μL, 30 μL; Covidien-Mallinckrodt) was added. After 30 minutes of incubation, labeling was validated using thin layer chromatography. In all cases, labeling efficacy was >99%. Before injection, saline (100 μL) was added.

Generation 4T1 tumor model

Cells were cultured under standard conditions in MEM medium containing MEM vitamins, l-glutamin, non-essential amino acids, natrium/pyruvate and penicillin/streptomycin solution (all BD Biosciences). Before transplantation, cells were trypsinized and washed with HBSS (BD Biosciences). For generation of the tumor lesions, 4T1-luc$^+$ tumor cells (0.25×10^5) were transplanted into the 4th mammary fatpad of Balb/c nude mice (n = 11; 6-8 weeks of age). All animal experiments were performed in accordance with Dutch welfare regulations and approved by the local ethics committee.

SPECT/CT imaging

Mice were injected intravenously with ^{111}In-MSAP-RGD (40 μg, 18 nmol, 10MBq) or ^{111}In-DTPA-RGD (25 μg, 25 nmol, 10 MBq). SPECT/CT scans were conducted as described previously on a preclinical SPECT/CT scanner (Nanospect; Bioscan) at 24 hr post injection.[18] CT images were used to provide anatomical reference to the location of the tumor and its metastases. Images were reconstructed and evaluated using identical settings and cut off values.

In vivo fluorescence imaging and biodistribution

Mice were sacrificed directly after SPECT/CT imaging and the blood was drawn by cardiac puncture. *In vivo* fluorescence images of ^{111}In-MSAP-RGD injected mice were recorded using the standard Cy5.5 settings (λ_{ex}=615-665, λ_{em}=695-770) of the IVIS 200 (Caliper LifeSciences). After dissection of the skin, the abdomen was covered to exclude the autofluorescence from this region. Next the organs were surgically removed and the fluorescence originating from these tissues was measured (photons/s/cm^2/sr) (Cy5.5 settings). Quantification was performed using Living Image 3D software package (Caliper LifeSciences). The biodistribution of ^{111}In-DTPA-RGD and ^{111}In-MSAP-RGD was determined by measuring the amount of radioactivity present in the organs, using a gamma counter (Wizard 3” 1480 automatic gamma counter, Perkin Elmer; 245kev; 60sec). Counts per minute were converted into MBq and corrected for decay. The percentage of the injected dose per gram of tissue (%ID/g) was calculated as followed: ((MBq measured in tissue/ injected dose) *100%)/weight of tissue.

Immunohistochemistry of (functional) blood vessels and H&E staining

To stain the functional vascularization of the tumor, fluorescein isothiocyanate-conjugated Lycopersicon esculentum (tomato) lectin (FITC-lectin) (Vector laboratories) was injected intravenously into the tail vein of one mouse and was allowed to circulate for 5 minutes. Afterwards the mouse was euthanized and perfused for 5 minutes with PBS via the left ventricle at a constant speed of 3 mL/min. Subsequently, tumors were removed and snap-frozen in liquid nitrogen. Cryosections were cut at 7 μm and adhered to StarFrost Microscope Slides (Knittel Glass). Slides were stored at -80 °C until use. For visualizing the total amount of present blood vessels, tumor tissue was immunostained with an antibody

against mouse-CD31. Slides were fixed for 10 minutes in acetone at -20 °C, rinsed twice in PBS and aspecific binding was blocked by incubation for 20 minutes with serum-free ProteinBlock (Dako Cytomation). Next, the slides were incubated o/n with a primary rat-anti-mouse CD31 antibody (PECAM-1, BD Biosciences Pharmingen), diluted 1:50 in 1% BSA in PBS, at 4 °C. After that, slides were washed 3 times with PBS and incubated for 1 hr with an AlexaFluor 594 labeled secondary rabbit-anti-rat IgG (H+L) (Invitrogen) 1:100 diluted in 1% BSA in PBS, at room temperature. Slides were washed again 3 times with PBS and mounted with Vectashield Mounting Medium for Fluorescence (Vector laboratories). Coverslips were sealed with nail polish and the slides were stored in the dark at 4 °C. For visualizing the accumulation of MSAP-RGD, slides with tumor tissue were sealed untreated and photographs were taken on a confocal microscope (Leica Microsystems CMS GmbH). Tissue morphology was examined by standard H&E-staining.

Supplementary Material

Refer to Web version on PubMed Central for supplementary material.

Acknowledgments

This research is supported by a Koningin Wilhelmina Fonds (KWF) translational research award (Grant No. PGF 2009-4344; FvL), an NWO VIDI-Grant (STW BGT 11271; FVL), and by NIH grants R01 EB009691 and EB011996 (LJ). This research is performed within the framework of the Centre for Translational Molecular Medicine (www.ctmm.nl) project MUSIS (AB), and within the FP7-project hyper image (TB).

References

1. van der Meel R, Gallagher WM, Oliveira S, O'Connor AE, Schiffelers RM, Byrne AT. Drug Discov Today. 2010; 15:102–114. [PubMed: 20035896]
2. Lucignani G, Larson SM. Eur J Nucl Med Mol Imaging. 2010; 37:1032–1038. [PubMed: 20352209]
3. Kenny LM, Coombes RC, Oulie I, Contractor KB, Miller M, Spinks TJ, McParland B, Cohen PS, Hui AM, Palmieri C, Osman S, Glaser M, Turton D, Al-Nahhas A, Aboagye EO. J Nucl Med. 2008; 49:879–886. [PubMed: 18483090]
4. Schottelius M, Laufer B, Kessler H, Wester HJ. Acc Chem Res. 2009; 42:969–980. [PubMed: 19489579]
5. Holm PW, Slart RH, Zeebregts CJ, Hillebrands JL, Tio RA. Ann Med. 2009; 41:257–264. [PubMed: 19089693]
6. Hermus L, Lefrandt JD, Tio RA, Breek JC, Zeebregts CJ. Atherosclerosis. 2010; 213:21–29. [PubMed: 20627248]
7. Hermus L, van Dam GM, Zeebregts CJ. Eur J Vasc Endovasc Surg. 2010; 39:125–133. [PubMed: 20031452]
8. ten Kate GL, Sijbrands EJ, Valkema R, ten Cate FJ, Feinstein SB, van der Steen AF, Daemen MJ, Schinkel AF. J Nucl Cardiol. 2010; 17:897–912. [PubMed: 20552308]
9. Zhu L, Niu G, Fang X, Chen X. Q J Nucl Med Mol Imaging. 2010; 54:291–308. [PubMed: 20639815]
10. Yang X. Radiology. 2010; 254:651–654. [PubMed: 20177082]
11. Schaafsma BE, Mieog JSD, Hutteman M, van der Vorst JR, Kuppen PJK, Lowik CWGM, Frangioni JV, van de Velde CJH, Vahrmeijer AL. J Surg Oncol. 2011; 104:323–332. [PubMed: 21495033]
12. Mieog JS, Troyan SL, Hutteman M, Donohoe KJ, van der Vorst JR, Stockdale A, Liefers GJ, Choi HS, Gibbs-Strauss SL, Putter H, Gioux S, Kuppen PJ, Ashitate Y, Lowik CW, Smit VT, Oketokoun R, Ngo LH, van de Velde CJ, Frangioni JV, Vahrmeijer AL. Ann Surg Oncol. 2011; 18:2483–2491. [PubMed: 21360250]
13. Celli JP, Spring BQ, Rizvi I, Evans CL, Samkoe KS, Verma S, Pogue BW, Hasan T. Chem Rev. 2010; 110:2795–2838. [PubMed: 20353192]

14. van Dam GM, Themelis G, Crane LMA, Harlaar NJ, Pleijhuis RG, Kelder W, Sarantopoulos A, de Jong JS, Arts HJG, van der Zee AGJ, Bart J, Low PS, Ntziachristos V. Nature Medicine. 2011; 17:1315–1319.
15. Stummer W, Pichlmeier U, Meinel T, Wiestler OD, Zanella F, Reulen HJ. Lancet Oncol. 2006; 7:392–401. [PubMed: 16648043]
16. Parker N, Turk MJ, Westrick E, Lewis JD, Low PS, Leamon CP. Anal Biochem. 2005; 338:284–293. [PubMed: 15745749]
17. Jennings LE, Long NJ. Chem Comm. 2009:3511–3524. [PubMed: 19521594]
18. van Leeuwen AC, Buckle T, Bendle G, Vermeeren L, Valdes Olmos R, van der Poel HG, van Leeuwen FWB. J Biomed Opt. 2011; 16:016004. [PubMed: 21280910]
19. Buckle T, van Leeuwen AC, Chin PT, Janssen H, Muller SH, Jonkers J, van Leeuwen FWB. Nanotechnology. 2010; 21:355101. [PubMed: 20689167]
20. van der Poel HG, Buckle T, Brouwer OR, Valdes Olmos RA, van Leeuwen FWB. Eur Urol. 2011; 60:826–833. [PubMed: 21458154]
21. Brouwer OR, Klop WMC, Buckle T, van den Brekel MWM, Balm AJM, Nieweg OE, Valdés-Olmos RA, van Leeuwen FWB. Ann Surg Oncol. 2011 accepted for publication. 10.1245/s10434-011-2180-7
22. Buckle T, Brouwer OR, Valdes Olmos R, van der Poel HG, Van Leeuwen FWB. J Nucl Med. 2012 accepted for publication.
23. Kuil J, Velders AH, van Leeuwen FWB. Bioconjug Chem. 2010; 21:1709–1719. [PubMed: 20812730]
24. Sampath L, Kwon S, Ke S, Wang W, Schiff R, Mawad ME, Sevick-Muraca EM. J Nucl Med. 2007; 48:1501–1510. [PubMed: 17785729]
25. Sirk SJ, Olafsen T, Barat B, Bauer KB, Wu AM. Bioconjug Chem. 2008; 19:2527–2534. [PubMed: 19053310]
26. Houston JP, Ke S, Wang W, Li C, Sevick-Muraca EM. J Biomed Opt. 2005; 10:054010. [PubMed: 16292970]
27. Li C, Wang W, Wu Q, Ke S, Houston J, Sevick-Muraca E, Dong L, Chow D, Charnsangavej C, Gelovani JG. Nucl Med Biol. 2006; 33:349–358. [PubMed: 16631083]
28. Garanger E, Aikawa E, Reynolds F, Weissleder R, Josephson L. Chem Commun. 2008:4792–4794.
29. Ye Y, Bloch S, Xu B, Achilefu S. Bioconjug Chem. 2008; 19:225–234. [PubMed: 18038965]
30. Edwards WB, Akers WJ, Ye Y, Cheney PP, Bloch S, Xu B, Laforest R, Achilefu S. Mol Imaging. 2009; 8:101–110. [PubMed: 19397855]
31. Haubner R, Gratias R, Diefenbach B, Goodman SL, Jonczyk A, Kessler H. J Am Chem Soc. 1996; 118:7461–7472.
32. Mas-Moruno C, Rechenmacher F, Kessler H. Anti-cancer agents Med Chem. 2010; 10:753–768.
33. van Hagen PM, Breeman WA, Bernard HF, Schaar M, Mooij CM, Srinivasan A, Schmidt MA, Krenning EP, de Jong M. Int J Cancer. 2000; 90:186–198. [PubMed: 10993959]
34. Raghunand N, Gatenby RA, Gillies RJ. Br J Radiol. 2003; 76(Spec No 1):S11–22. [PubMed: 15456710]
35. Cai W, Chen K, Li ZB, Gambhir SS, Chen X. J Nucl Med. 2007; 48:1862–1870. [PubMed: 17942800]
36. Boswell CA, Eck PK, Regino CA, Bernardo M, Wong KJ, Milenic DE, Choyke PL, Brechbiel MW. Mol Pharm. 2008; 5:527–539. [PubMed: 18537262]
37. Berezin MY, Guo K, Akers W, Livingston J, Solomon M, Lee H, Liang K, Agee A, Achilefu S. Biochem. 2011; 50:2691–2700. [PubMed: 21329363]
38. Bunschoten A, Buckle T, Kuil J, Luker GD, Luker KE, Nieweg OE, van leeuwen FWB. Biomaterials. 2012; 33:867–875. [PubMed: 22024362]
39. Buckle T, Chin PTK, van Leeuwen FWB. Nanotechnology. 2010; 21:482001. [PubMed: 21063057]
40. Kuil J, Buckle T, Yuan H, Oishi S, Fujii N, Josephson L, van Leeuwen FWB. Bioconjug Chem. 2011; 22:859–864. [PubMed: 21480671]

41. Kuil J, Buckle T, Oldenburg J, Yuan H, Borowsky AD, Josephson L, Van Leeuwen FWB. Mol Pharm. 2011; 8:2444–2453. [PubMed: 22085282]
42. Shao F, Yuan H, Josephson L, Weissleder R, Hilderbrand SA. Dyes and Pigments. 2011; 90:119–122. [PubMed: 21475610]
43. Garanger E, Blois J, Hilderbrand SA, Shao F, Josephson L. J Comb Chem. 2010; 12:57–64. [PubMed: 19928910]

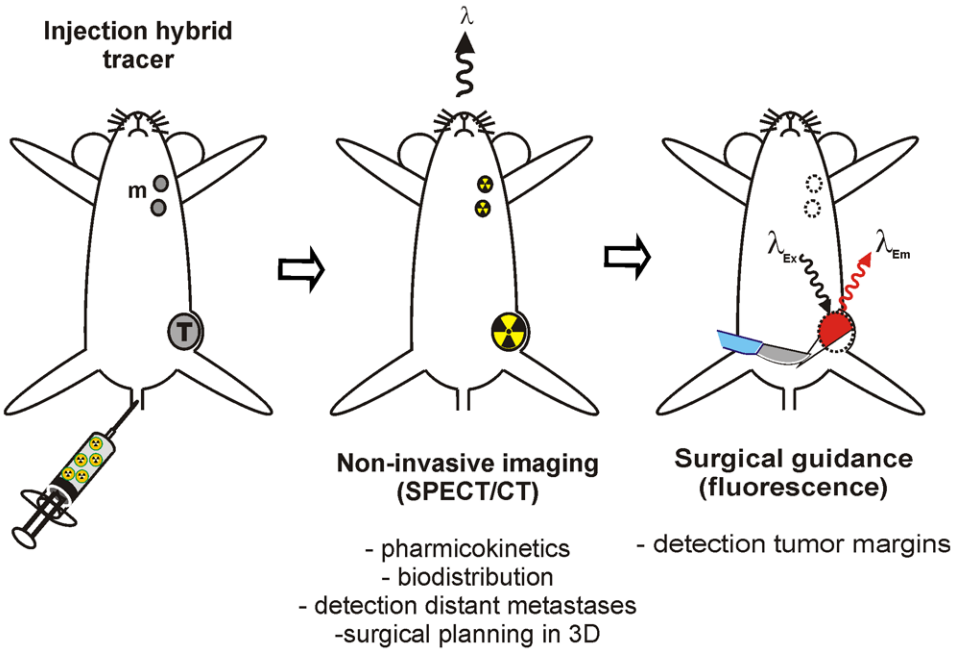

Figure 1.
Hybrid tumor-targeting approach. Injection of a hybrid tumour targeted agent allows preoperative nuclear imaging and intraoperative image guided surgery

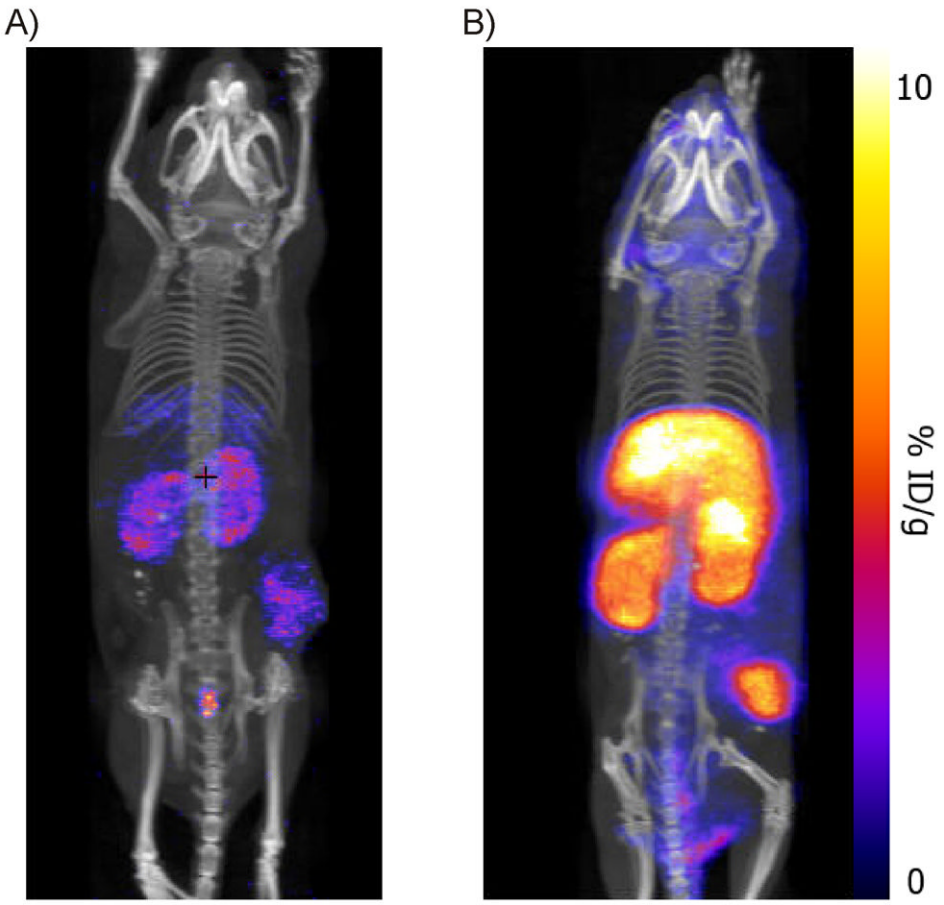

Figure 2.
A) MIP SPECT/CT image obtained with ^{111}In-DTPA-RGD, B) MIP SPECT/CT with ^{111}In-MSAP-RGD. Due to the higher retention of the tracer at 24h the accumulation in B is more intense when both tracers are imaged with identical settings (see also Table 1)

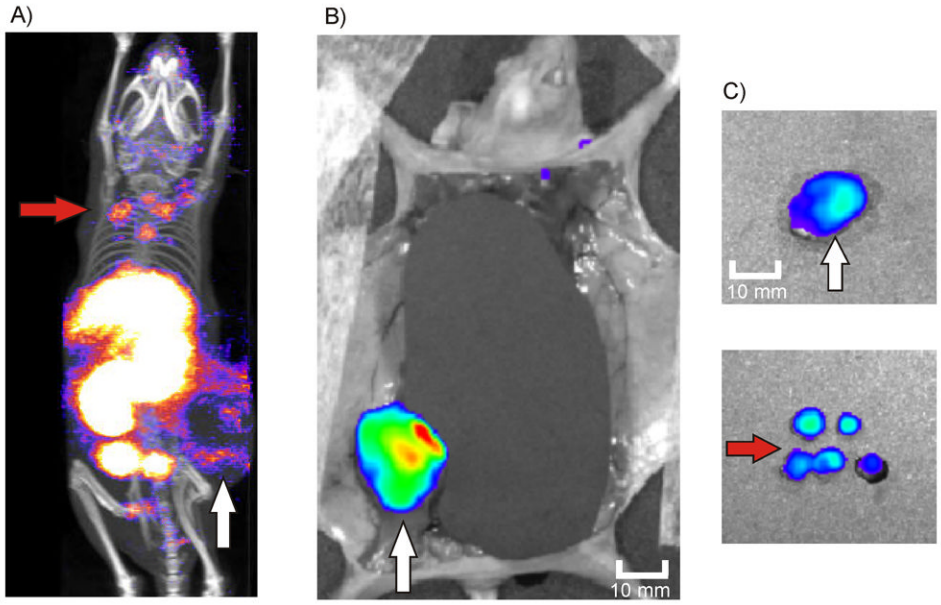

Figure 3.

Surgical guidance towards the tumor margins of the primary tumor and distant metastases after injection of ^{111}In-MSAP-RGD. A) Planning SPECT/CT image depicting both the rim of the primary tumor and distant metastases in the neck area (mouse belly down), B) Fluorescence imaging (organs are shielded) depicting the margins of the primary tumor (mouse belly up), C) Ex vivo fluorescence imaging of the tumor and distant metastases

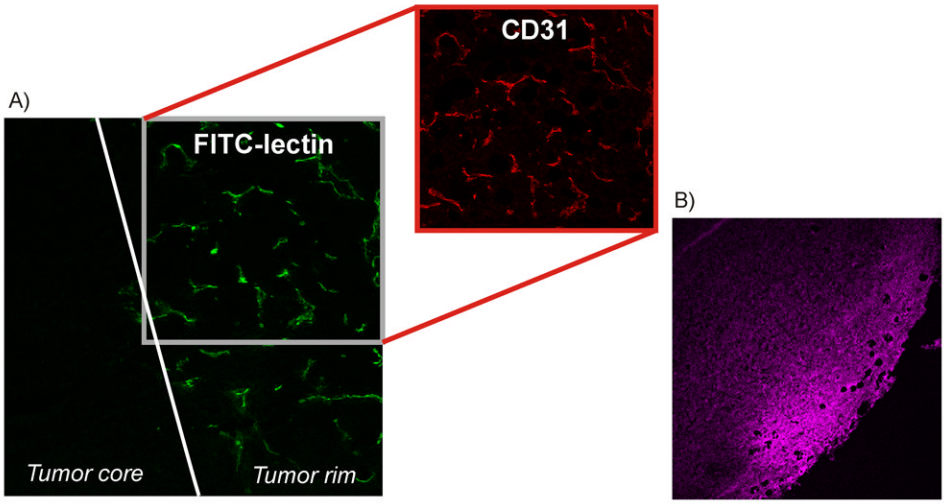

Figure 4.

Tumor tissue ex vivo, demonstrating tumor vascularity, viability and distribution of ^{111}In-DTPA-RGD A) perfusion of the tumor rim visualized with Fitc-lectin perfusion and incubation with a rat-anti-mouse CD31 antibody followed by an AlexaFluor 594 labeled rabbit-anti-rat antibody (20×), B) Fluorescence imaging (λ_{em}633nm) of MSAP-RGD in the tumor rim 24h after iv injection (10×)

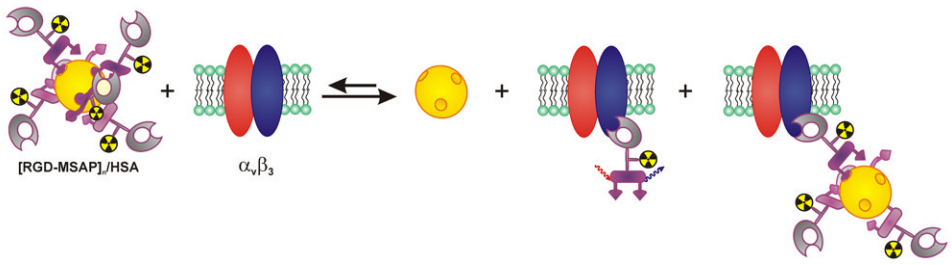

Figure 5.
The non-covalent interaction of MSAP-RGD is reversible and the equilibrium can be shifted to the right side by interactions with $\alpha_v\beta_3$-integrins and alternative (non-specific) binding sites.

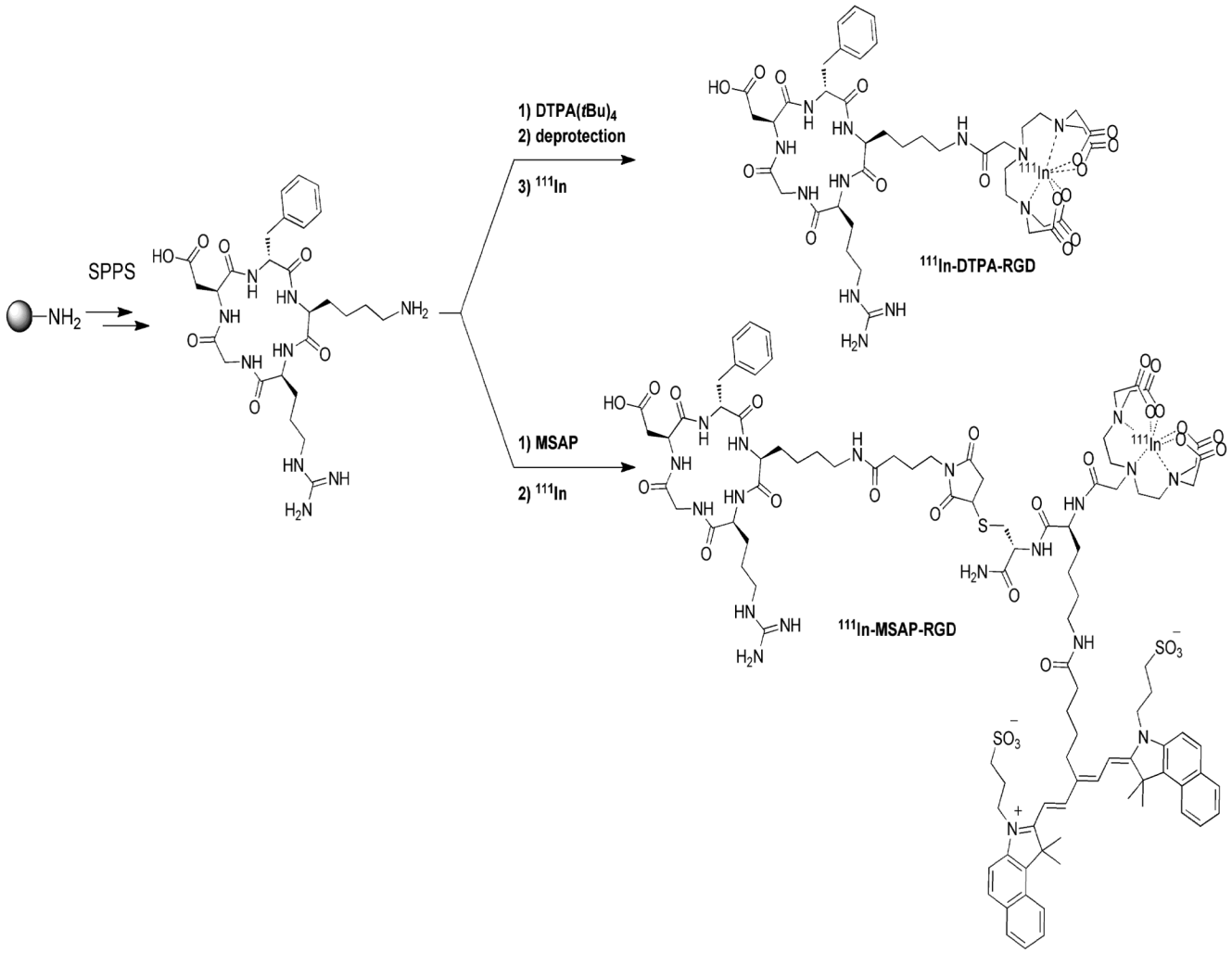

Scheme 1.
Synthesis and radiolabeling of DTPA-RGD and MSAP-RGD

Table 1

Biodistribution of ^{111}In-DTPA-RGD and ^{111}In-MSAP-RGD at 24h post iv injection

	^{111}In-DTPA-RGD (% ID/g)[a]	^{111}In-MSAP-RGD (% ID/g) [a]	Ratio MSAP-RGD/DTPA-RGD	^{99m}Tc-HSA (% ID/g)[b]
Blood	0.03 (±0.01)	0.13 (±0.02)	5.2	3.74 (±0.21)
Brain	0.02 (±0.03)	0.05 (±0.01)	2.1	0.10 (±0.01)
Lungs	0.07 (±0.02)	1.00 (±0.29)	14.0	1.80 (±0.43)
Heart	0.03 (±0.01)	0.70 (±0.12)	22.6	1.31 (±0.24)
Liver	0.27 (±0.10)	4.87 (±1.17)	17.9	1.98 (±0.16)
Kidneys	0.78 (±0.10)	9.26 (±1.40)	11.8	3.83 (±0.25)
Spleen	0.17 (±0.08)	1.61 (±0.60)	10.6	1.52 (±0.16)
Stomach	0.07 (±0.02)	0.69 (±0.21)	10.4	0.81 (±0.13)
Intestines	0.09 (±0.02)	0.98 (±0.24)	11.1	1.83 (±0.12)
Muscle (paw)	0.03 (±0.01)	0.31 (±0.08)	12.1	0.27 (±0.13)
Fat (neck)	0.02 (±0.01)	0.28 (±0.12)	11.1	0.48 (±0.04)
Mammary gland	0.03 (±0.01)	0.25 (±0.10)	8.3	0.68 (±0.40)
Inguinal LN	0.04 (±0.02)	0.42 (±0.27)	11.7	0.81 (±0.22)
Axilary LN	0.12 (±0.06)	0.98 (±0.33)	8.5	1.86 (±0.26)
Tumor	0.26 (±0.03)	2.59 (±0.55)	10.0	n.d.
T/M ratio	11.11 (±4.16)	9.03 (±3.81)		

[a] n=5,

[b] n=3; data given as average (±SD)